

The Large-Angle Photon Veto System for the NA62 Experiment at CERN

F. Ambrosino, B. Angelucci, A. Antonelli, F. Costantini, G. D'Agostini, D. Di Filippo, R. Fantechi, S. Gallorini, S. Giudici, E. Leonardi, I. Mannelli, P. Massarotti, M. Moulson*, M. Napolitano, V. Palladino, F. Rafaelli, M. Raggi, G. Saracino, M. Serra, T. Spadaro, P. Valente, S. Venditti

Abstract—The branching ratio (BR) for the decay $K^+ \rightarrow \pi^+ \nu \bar{\nu}$ is a sensitive probe for new physics. The NA62 experiment at the CERN SPS will measure this BR to within about 10%. To reject the dominant background from channels with final state photons, the large-angle vetoes (LAVs) must detect photons of energy as low as 200 MeV with an inefficiency of less than 10^{-4} , as well as provide energy and time measurements with resolutions of 10% and 1 ns for 1 GeV photons. The LAV detectors make creative reuse of lead glass blocks recycled from the OPAL electromagnetic calorimeter barrel. We describe the mechanical design and challenges faced during construction, the characterization of the lead glass blocks and solutions adopted for monitoring their performance, and the development of front-end electronics to allow simultaneous time and energy measurements over an extended dynamic range using the time-over-threshold technique. Our results are based on test-beam data and are reproduced by a detailed Monte Carlo simulation that includes the readout chain.

Index Terms—Calorimetry, Detectors, Elementary particles

I. THE NA62 EXPERIMENT

The decays $K^+ \rightarrow \pi^+ \nu \bar{\nu}$ and $K_L \rightarrow \pi^0 \nu \bar{\nu}$ are flavor-changing neutral-current processes whose amplitudes are dominated by Z-penguin and box diagrams. Because there are no contributions from long-distance processes with intermediate photons and because the hadronic matrix elements can be obtained from rate and form factor measurements for common $K \rightarrow \pi \ell \nu_\ell$ decays, the branching ratios (BRs) for the $K \rightarrow \pi \nu \bar{\nu}$ decays can be calculated in the Standard Model (SM) with minimal intrinsic uncertainty (see Ref. 1 for a recent review). The BRs for these decays are therefore a sensitive probe of the SM flavor sector and provide constraints on the CKM unitarity triangle that are complementary to those from measurements of B -meson decays.

On the other hand, the tiny BRs for these decays are notoriously difficult to measure, not least because of the

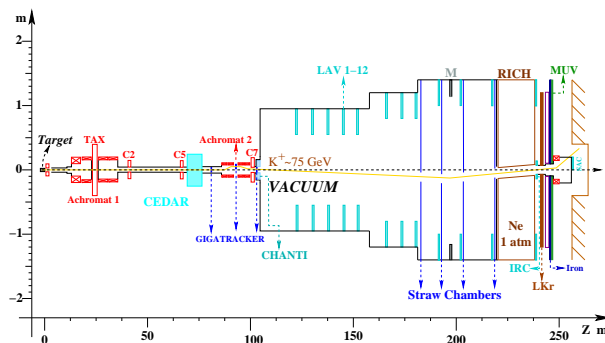


Fig. 1. The NA62 experimental layout.

three-body kinematics with two undetectable neutrinos in the final state. At present, the experimental value of the BR for the decay $K^+ \rightarrow \pi^+ \nu \bar{\nu}$ is $1.73^{+1.15}_{-1.05} \times 10^{-10}$ on the basis of seven detected candidate events [2]. The goal of NA62, an experiment at the CERN SPS, is to detect ~ 100 $K^+ \rightarrow \pi^+ \nu \bar{\nu}$ decays with a S/B ratio of 10:1 in two years of data taking beginning in 2013. The experiment is fully described in Ref. 3. The experimental layout is illustrated in Fig. 1.

NA62 will make use of a 75-GeV unseparated positive secondary beam with a total rate of nearly 800 MHz, of which ~ 50 MHz is K^+ 's. The K^+ 's are identified by the CEDAR differential Cerenkov counter in the beamline. All 800 MHz of beam particles are tracked by three silicon-pixel tracking detectors (the Gigatracker) located at the achromat just upstream of the vacuum decay volume, providing event-by-event measurements of the K^+ trajectory and momentum. The decay volume is evacuated to 10^{-6} mbar in order to minimize background between interactions and residual gases. It begins ~ 100 m downstream of the production target, is ~ 110 m long, and consists of segments of increasing diameter, from ~ 2 m upstream to ~ 3 m downstream. 5 MHz of kaon decays are observed in the 65-m fiducial decay region, in the upstream part of the vacuum tank. The ring-shaped large-angle photon vetoes (LAVs) are placed at 11 stations along the vacuum volume and provide full coverage for decay photons with $8.5 \text{ mrad} < \theta < 50 \text{ mrad}$. The last 35 m of the vacuum volume host a dipole spectrometer with four straw-tracker stations operated in the vacuum. At the exit of the vacuum region, a ring-imaging Cerenkov counter (RICH) 4 m in diameter by 17 m in length helps to identify charged decay secondaries. Downstream of the RICH, a number of photon vetoes provide hermeticity, including principally

Manuscript received November 15, 2011.

F. Ambrosino, D. Di Filippo, P. Massarotti, M. Napolitano, and G. Saracino are with the Dipartimento di Scienze Fisiche dell'Università and Sezione INFN, Napoli, Italy.

B. Angelucci, F. Costantini, R. Fantechi, S. Gallorini, S. Giudici, I. Mannelli, F. Rafaelli, and S. Venditti are with the Dipartimento di Fisica dell'Università and Sezione INFN, Pisa, Italy.

A. Antonelli, M. Moulson, M. Raggi, and T. Spadaro are with the Laboratori Nazionali di Frascati dell'INFN, Frascati, Italy.

G. D'Agostini, E. Leonardi, V. Palladino, M. Serra, and P. Valente are with the Dipartimento di Fisica dell'Università "La Sapienza" and Sezione INFN, Roma, Italy.

*Presenter. Address correspondence to Matthew Moulson, e-mail: moulson@lnf.infn.it

the NA48 liquid-krypton calorimeter (LKr) to veto forward ($1 \text{ mrad} < \theta < 8.5 \text{ mrad}$), high-energy photons. The 12th LAV station provides downstream coverage at large angles ($8.5 \text{ mrad} < \theta < 50 \text{ mrad}$), while a ring-shaped shashlyk calorimeter (IRC) about the beamline provides coverage for photons with $\theta < 1 \text{ mrad}$. Further downstream, a muon veto detector (MUV) provides additional rejection for $K \rightarrow \mu \nu$ events, and a small-angle shashlyk calorimeter (SAC) around which the beam is deflected completes the coverage for very-small-angle photons that would otherwise escape via the beam pipe.

Assuming an acceptance for signal events of about 10%, the experiment must be able to reject background from the dominant K^+ decays such as $K^+ \rightarrow \pi^+ \pi^0$ at the level of 10^{12} . Kinematic cuts on the K^+ and π^+ tracks (as reconstructed in the Gigatracker and straw chambers, respectively) provide a rejection factor of 10^4 and ensure that the photons from the π^0 have 40 GeV of energy. There is a kinematic correlation between photon energy and angle of emission with respect to the beam axis; the forward photons that are intercepted by the LKr calorimeter, IRC, and SAC have much higher energies than those intercepted by the LAVs. Nevertheless, the photons from $K^+ \rightarrow \pi^+ \pi^0$ intercepted by the LAVs may have energies from a few tens of MeV to several GeV. In order to detect the π^0 with an inefficiency of $\leq 10^{-8}$, the maximum tolerable inefficiency in the LAV detectors for photons with energies as low as 200 MeV is 10^{-4} . In addition, the LAV detectors must have good time resolution ($\sim 1 \text{ ns}$) to allow signals from incident particles to be identified with the correct event, and good energy resolution ($\sim 10\%$ at 1 GeV) for precise vetoing and use in full-event reconstruction. The system must also be sensitive to minimum-ionizing particles. Finally, the LAV detectors must be compatible with operation in a vacuum of 10^{-6} mbar .

II. THE LARGE-ANGLE VETO SYSTEM

The NA62 LAV detectors make creative reuse of lead glass blocks recycled from the OPAL electromagnetic calorimeter barrel [4], which became available in 2007, when various technologies were under consideration for the construction of the LAV detectors. Other solutions considered included a lead/scintillating tile design originally proposed for use in the (later canceled) CKM experiment at Fermilab, and a lead/scintillating-fiber design based on the electromagnetic calorimeter for the KLOE experiment. Prototype instruments based on each of the three technologies were obtained or constructed, and tested with the electron beam at the Frascati Beam-Test Facility. These tests demonstrated that all three technologies are suitable for use in NA62 [5]. In particular, the inefficiency for the detection of single, tagged electrons with the OPAL lead glass modules was measured to be $1.2^{+0.9}_{-0.8} \times 10^{-4}$ at 203 MeV and $1.1^{+1.9}_{-0.7} \times 10^{-5}$ at 483 MeV. Basing the construction of the LAV system on the OPAL lead glass modules provides significant economic advantages.

The modules from the central part of the OPAL electromagnetic calorimeter barrel consist of blocks of Schott SF57 lead glass. This material is about 75% lead oxide by weight and has

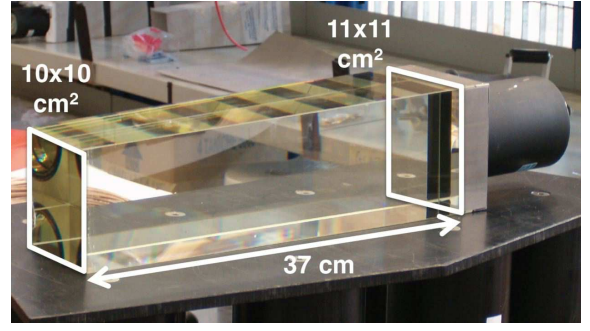


Fig. 2. A module from the OPAL calorimeter, without wrapping and with reinforcement plates at the interface between the glass and the steel flange.

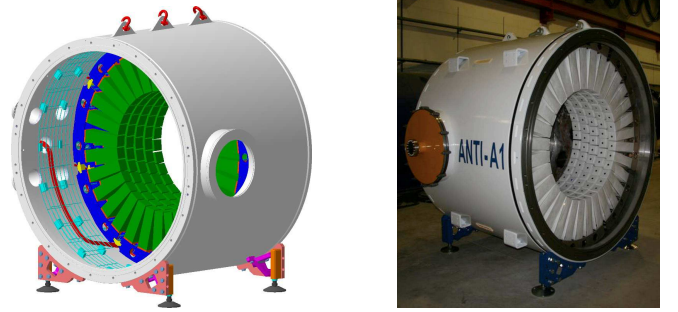


Fig. 3. Design study (left) and completed prototype A1 veto station (right) making use of the OPAL lead glass calorimeter elements.

a density $\rho = 5.5 \text{ g/cm}^3$ and a radiation length $X_0 = 1.50 \text{ cm}$; its index of refraction is $n \approx 1.85$ at $\lambda = 550 \text{ nm}$ and $n \approx 1.91$ at $\lambda = 400 \text{ nm}$. Electromagnetic showers in the lead glass are detected by virtue of the Cerenkov light produced; our measurements indicate that, averaged over modules, minimum ionizing particles produce about 0.34 p.e. per MeV of deposited energy. The front and rear faces of the blocks measure about $10 \times 10 \text{ cm}^2$ and $11 \times 11 \text{ cm}^2$, respectively; the blocks are 37 cm in length. (The precise geometry depends slightly on the ring of the OPAL calorimeter from which each block is extracted; blocks of uniform geometry are used in the construction of each ring of the LAV system.) Each block is read out at the back side by a Hamamatsu R2238 76-mm PMT, which is optically coupled via a 4-cm long cylindrical light guide of SF57 of the same diameter as the PMT. The rear face of the glass block is glued to a 1-cm thick stainless steel flange featuring the holes that allow mounting hardware to be attached and a circular cutout for the light guide. A mu-metal shield surrounding the PMT and light guide is also glued to the flange. A complete module (block plus PMT) is a monolithic assembly; the block and PMT cannot be independently replaced. Figure 2 shows a picture of a complete module.

A LAV station is made by arranging these blocks around the inside of a segment of vacuum tank, with the blocks aligned radially to form an inward-facing ring. Multiple rings are used in each station in order to provide the desired depth for incident particles. The blocks in successive rings are staggered in azimuth; the rings are spaced longitudinally by about 1 cm.

The LAV system consists of a total of 12 stations, the

TABLE I
PARAMETERS OF LAV STATIONS

Station	Diameter [mm]		Block radius [mm]		Layers	Blocks
	Outer wall		Inner	Outer		
A1–A5	2168		537	907	5	160
A6–A8	2662		767	1137	5	240
A9–A11	3060		980	1350	4	240
A12	~3250		1072	1442	4	256

diameter of which increases with distance from the target. The geometry of the LAV stations is summarized in Table I. For stations A1–A5, A6–A8, and A9–A11, apart from the different sizes and block configurations, the designs are conceptually similar. The geometry of A12 is not yet final; this station is operated in air and its design is different from that of the other stations. Since the spaces between the blocks are significantly smaller in the larger-diameter vessels, fewer layers are necessary. As a result of the staggering scheme, particles incident on any station are intercepted by blocks in at least three rings, for a total minimum effective depth of 21 radiation lengths. The vast majority of incident particles are intercepted by four or more blocks ($27 X_0$). The stations with five layers (A1–A8) are 1.55 m in length, while those with four layers (A9–11) are 1.43 m in length.

Station A1 was constructed as a prototype during the first half of 2009. It was installed in the NA62 beamline at CERN and tested with electrons and muons in October 2009. The design study and completed station are shown in Fig. 3. On the basis of experience gained during the test beam, various improvements were made. Station A2 was then constructed and tested with an unseparated, low-energy positive beam in the T9 beamline at the CERN PS in August 2010. A1 was subsequently rebuilt to incorporate the design improvements. Construction of the remaining stations was then commenced and is now underway.

III. LAV CONSTRUCTION

The LAV vacuum vessels are constructed from 25-mm thick steel plate, rolled into a cylinder and arc welded along the seam. Structural steel (S275JR) is used for stations A1 to A8 and A11. Stations A9 and A10 are mounted astride the spectrometer magnet, so non-magnetic ($\mu/\mu_0 \approx 1.01$) 304L stainless steel is used for these stations. After rolling, seam welding, and welding of the end flanges, the interior is turned on a vertical lathe and the vessel is vacuum tested. Five 200-mm ISO-F flanges for HV, signal, and calibration connections are welded via nozzles 20-cm long to one side of the vessel. One 630-mm ISO-K flange is attached to the opposite side for use as a manhole; the pumps for the NA62 vacuum system are also mounted on these flanges. Bolt holes on the flanges and in the interior walls of the tank are drilled with a CNC milling machine. A final vacuum test is performed, the residual magnetic field is mapped, and the chamber is cleaned and the outside is painted. A passivator that does not interfere with high-vacuum operation is applied to the inside walls of the vessel. The contract for the construction of vessels A1

to A8 and A11 was awarded to Fantini SpA (Anagni, Italy). Construction of A1 to A7 has been completed; construction of A8 is in progress.

The OPAL detector modules (lead glass block plus PMT) were manufactured by Hamamatsu during the mid-1980s. Their recycling requires substantial care throughout the assembly procedure.

After the storage area in which the modules were kept was inundated during a flash flood in spring 2008, the modules were subject to an extensive sorting and clean-up effort carried out at CERN by an industrial recovery firm. They were subsequently shipped to Frascati for use in LAV assembly.

The interface between the stainless steel flange and lead glass block is fragile, and is found to be critically damaged in a few percent of the modules upon first examination. Typically, the epoxy between the glass and steel is found to have become delaminated in some areas, while in others, the glass is fractured at the interface with pieces still adhering to the flange. This is attributed to thermally induced stress from the differing expansion coefficients of the steel and of the glass and/or thermal shock in the glass due to the conductivity of the flange. Some modules are found to have the glass block completely separated from the steel flange. Since the modules are suspended by the flange in the LAV system, the fragility of the interface is a structural vulnerability and a safety risk. The first step in the processing of the modules at Frascati is to therefore to reinforce the interface. Using epoxy resin, 20 cm² \times 0.5-mm thick stainless steel plates are attached across the glass-steel interface on all four sides of the block. Calculations indicate and static tests confirm that the reinforced bond is several times stronger than the original bond.

To maintain the design vacuum of $\sim 10^{-6}$ mbar, all components of the LAV detectors must be carefully cleaned. A variety of techniques are used, including pickling, solvent degreasing, and ultrasonic cleaning. The lead glass blocks require special care. After reinforcement of the glass/steel interface, the original wrapping is removed and the blocks are thoroughly cleaned with acetone or isopropyl alcohol. They are then wrapped with a new laser-cut and heat-welded Tyvek cover.

During the A1 test beam, ringing of the analog signal was observed to lead to errors in charge reconstruction using the time-over-threshold technique discussed below. This problem was traced to a small parasitic inductance in the PMT dynodes and solved by replacing the original OPAL HV dividers soldered to the PMTs with new dividers of our own design. The new divider features additional resistors on the last three dynodes and anode to damp out the oscillation, storage capacitors for the last three dynode stages to improve response linearity for large signals, and a decoupling resistor between the HV and signal grounds to decrease noise.

After the divider is replaced, the blocks are tested and characterized 12 at a time using a test station featuring an LED pulser and cosmic-ray telescope (Fig. 4). The PMT gains are measured first, by varying the intensity of the light pulses from the LEDs as well as the PMT HV settings and mapping out the response for each block. Using the gain curves

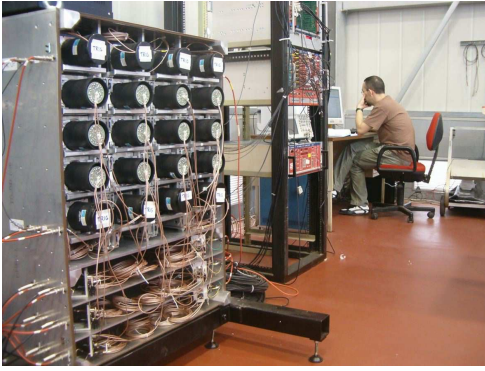


Fig. 4. Test stand used for the characterization of lead glass detector modules. The top and bottom rows of lead glass blocks form a telescope for the selection of vertical cosmic rays. Here, the front panel is open; it is closed during operation.

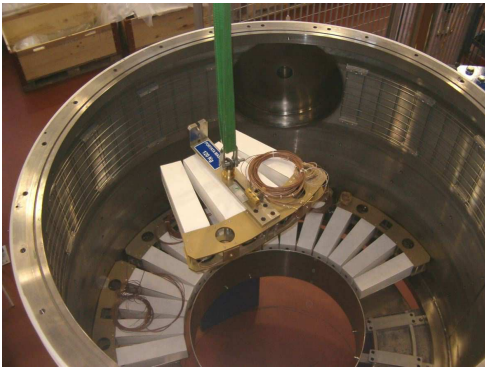


Fig. 5. Installation of lead glass modules into the steel vacuum vessel.

so obtained, the PMTs are then set to a reference value of the gain (9×10^5 or 1×10^6) and the response to cosmic rays selected by the telescope is measured; the photoelectron yield for the block (p.e./MeV) is then obtained assuming that vertically incident cosmic rays leave 77 MeV in each block. As noted above, photoelectron yields of 0.34 p.e./MeV are typical. Finally, using the gain curves and the measurements of photoelectron yield, the PMT voltages are set to the values expected to produce a common output charge level of 4.5 pC for cosmic ray events. The response is measured and the HV setting is validated. Thus, at the end of a 12-hour cycle, which is fully automated using LabView, we have PMT gain and photoelectron yield measurements as well as the operational HV settings for 12 modules. Additional data (current-draw measurements, dark-count rates) are also collected using the test station.

The OPAL design features an optical port at the base of each module. Blue LEDs are installed in these optical ports as part of the calibration and monitoring system, and will allow monitoring of the operational status and relative timing for each block. A low-capacitance LED was chosen to minimize the rise and fall times of the light pulse; this is important for use with the time-over-threshold-based readout system discussed in the following section. In principle, the LED system should allow in-situ gain measurement as well.

After testing and characterization, the blocks are arranged in groups of four in an aluminum mounting bracket. For

the installation, the vacuum vessel is turned on end. The aluminum mounting bracket with four modules is lowered into the upended vessel by overhead crane and bolted to the wall, as illustrated in Fig. 5. The HV, signal, and LED cables are then routed to the flanges along the cable grille visible at the top of the photo. In order to preserve uniformity of signal shapes and timing across channels, all signal (and LED) cables have the same length, with cable slack taken up on the grille. For HV cables, the excess length is cut.

As noted above, the signal, HV, and LED connections are made on five 200-mm ISO-F flanges. Flanges with eight or ten DB37 connectors are used both for signal and LED feed-through, 16 channels per connector, with separate ground connections for each signal channel. Flanges with eight 32-pin MIL-C-26482 connectors are used for HV feed-through, 32 channels per connector, with a common ground for all 32 channels on a separate MHV feedthrough.

IV. FRONT-END ELECTRONICS

As noted above, the LAVs must furnish time and energy measurements over a large range of incident photon energies. For reasons of cost and simplicity, we have decided on a read-out scheme based on the time-over-threshold (ToT) technique. This scheme is implemented using a dedicated front-end ToT discriminator board of our own design [6] and a digital readout board (TEL62) used by various NA62 detector subsystems [7]. The ToT discriminator converts the analog signals from the detector to low-voltage differential signal (LVDS) pulses, with width equal to the duration of the analog signal from the detector above a specified threshold. The signal from each PMT is compared to two different thresholds, a low threshold of about 5 mV and a high threshold expected to be about 50 mV, corresponding to two different LVDS outputs. (For comparison, the expected noise level is 2 mV under normal operating conditions.) The TEL62 is based on the design of the TELL1 readout board developed for the LHCb experiment. On the TEL62, TDC mezzanines measure the leading and trailing times of the LVDS pulses. Using a time-to-charge calibration parameterization, the FPGA on board the TEL62 calculates the time corrected for slewing, as well the charge for each hit as reconstructed from the pulse width above threshold. This information is sent to the subsequent DAQ stages. Level-0 trigger primitives are also calculated on board the TEL62 and sent to the level-0 trigger processor.

A conceptual schematic of the ToT discriminator board is presented in Fig. 6 to illustrate the signal processing for a single channel. Since each channel is discriminated against two different thresholds, the board has 32 input channels and 64 output channels.

While the amplitude of the PMT signal from a minimum ionizing particle is about 20 mV, signals from 20-GeV showers may be as large as 10 V. For protection, the input signal is clamped at 0.6 V by a circuit that maintains the timing of the rising and falling edges of the pulse. The clamped signal is then passively split. One copy of the signal is summed with the signals from other channels to form diagnostic analog outputs as discussed below. The other copy is amplified $\times 3$

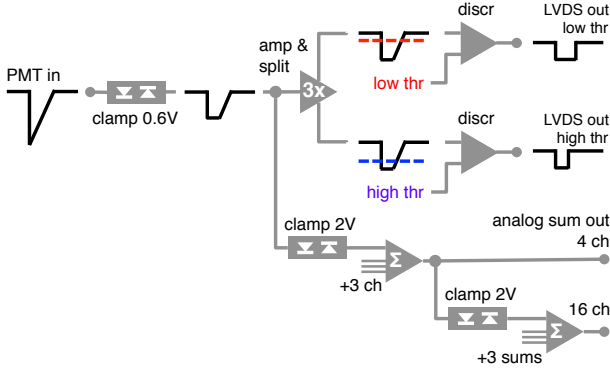


Fig. 6. Conceptual schematic of the ToT discriminator board.

by a low-noise, high-bandwidth, high-speed amplifier and passively split into two copies. Each copy is used as input to a high-speed comparator with an LVDS driver. The threshold for comparison is provided by a programmable DAC in the board controller. To reduce double pulses from the comparator due to noise in the input signal, 3 mV of hysteresis is also provided through a feedback resistor, so that the output signal is extended until the input signal falls to 3 mV below the threshold.

The other copy of the clamped analog signal is summed with the signals from three adjacent channels (and clamped at 2 V) for diagnostic purposes. The resulting analog sum is made available via a front-panel LEMO connector. These sums of four are in turn summed four at a time to produce sums of 16. For 32 input channels, there are a total of 10 front-panel analog outputs: eight sums of four and two sums of 16. A compact way to perform single channel diagnostics is to pulse the blocks one at a time using the LED system and read out the analog signal from these sums.

The readout board is implemented on a 9U VME card and has a modular structure, with many of the important functions on mezzanines, to reduce costs and simplify repairs. The ToT discriminators are implemented on 16 mezzanines, each with 4 discriminator circuits. The analog sums are handled on 10 mezzanines (one per front-panel output). A pulse-generator mezzanine allows pulses of programmable width and amplitude to be sent to a pattern of channels on the input connectors. The board controller mezzanine handles communication with the experiment's slow-control system to allow the thresholds to be set and read, to control the test-pulse generator, and to monitor the board status.

V. TEST-BEAM PERFORMANCE

The A2 LAV station was tested using the positive secondary beam in the T9 area at the CERN PS in August 2010. Data were collected at various beam momenta over the interval 0.3–10 GeV. The composition of the T9 beam changes as a function of the momentum setting. At 0.3 GeV, the beam is roughly 70% e^+ and 30% π^+ (including decay μ^+), while above 6 GeV the e^+ component drops off sharply and at 10 GeV the beam is roughly a 50% mix of π^+/μ^+ and p . Two threshold Cerenkov counters in the beamline using CO₂ at adjustable pressure allowed samples enriched e^+ and μ^+ to

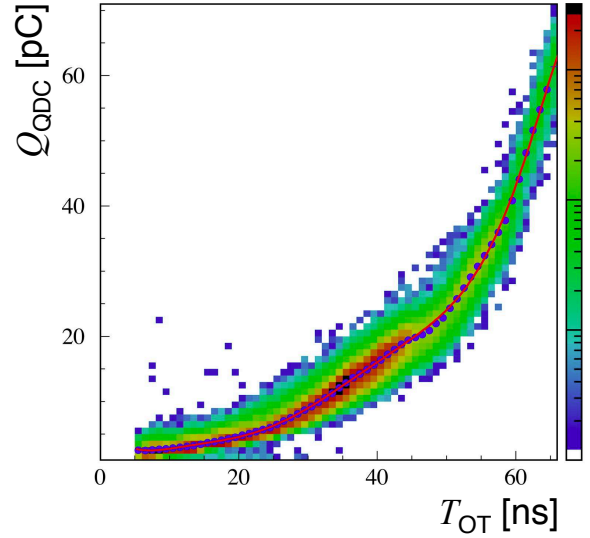


Fig. 7. Scatter plot of signal charge measured using the QDCs vs. signal time over threshold, for electrons of various energies at the T9 test beam.

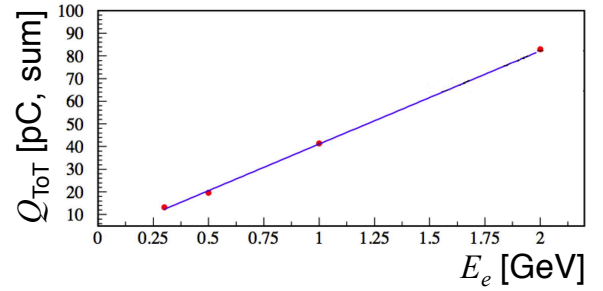


Fig. 8. Equivalent charge-integrated signal from ToT vs. incident electron energy, demonstrating linearity of response.

be selected. The T9 detectors also included two scintillation paddles and a beam wire chamber for beam counting and diagnostics. The beam focus was 2 m downstream of the beam wire chamber, and A2 was positioned so that the beam focus coincided approximately with the first layer of lead glass blocks. Two additional scintillator paddles ($60 \times 85 \text{ mm}^2$) were placed in a cross configuration at beam entrance and one larger paddle was placed at beam exit. Requirements on the signal amplitude for both entrance counters significantly enriched the sample in events with a single beam particle incident on a single column of lead-glass blocks, while requiring in addition a hit on the exit counter significantly enriched the sample in events in which the beam particle was a μ^+ . A prototype of the ToT discriminator board (with one discriminator per channel, rather than two) was tested together with A2. For much of the test, our board was used together with commercial QDCs and TDCs, but in dedicated runs, the times were also measured with a prototype setup using a TELL1 board from LHCb and an early version of the TDC mezzanine.

Figure 7 shows a scatter plot of the signal charge measured using the QDCs vs. the signal time over a threshold of 4 mV, for electrons. The data are summed for all blocks on which the beam was incident and over runs of different energies. For small signals, a small increase in the integrated charge corresponds to a large increase in the time over threshold; the

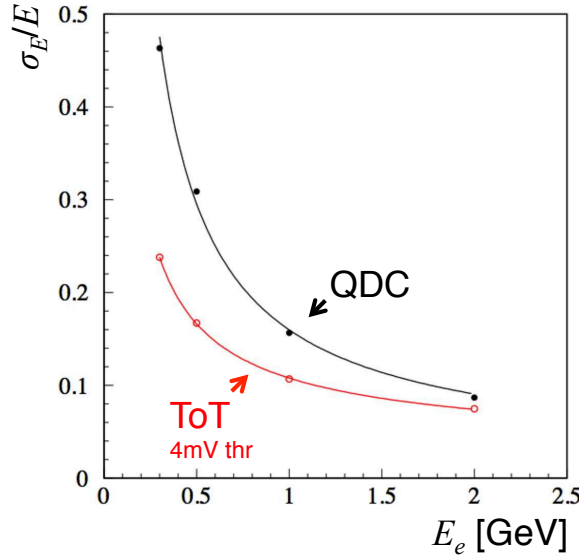


Fig. 9. Energy resolution obtained using the ToT technique compared with that obtained using the QDCs, as a function of incident electron energy.

ToT measurement provides more sensitivity for small signals than does the QDC measurement. This is a desirable property for the LAV detectors, since high detection efficiency is required for low-energy photons. Parameterizations of the type illustrated in Fig. 7 are used to convert the time over threshold to an effective charge measurement. Figure 8 demonstrates that good linearity of response is obtained using this method. The plot shows the equivalent charge in pC from the ToT measurement (with 4 mV threshold) for electrons of energy 0.3, 0.5, 1, and 2 GeV. Linearity to within 1% is observed. The energy resolution obtained using the ToT technique is compared with that obtained using the QDCs in Fig. 9. As expected from the form of the curve in Fig. 7, at low energies, the resolution obtained with the ToT technique is better than that obtained with the QDCs. The fits in Fig. 9 give

$$\begin{aligned} \text{QDC:} \quad \sigma_E/E &= 8.6\% / \sqrt{E [\text{GeV}]} \oplus 13\% / E, \\ \text{ToT:} \quad \sigma_E/E &= 9.2\% / \sqrt{E [\text{GeV}]} \oplus 5\% / E \oplus 2.5\%. \end{aligned}$$

While, as expected, the statistical contribution to the energy resolution is about the same with either readout scheme, the contribution from noise (term proportional to $1/E$) appears to be significantly smaller with the ToT technique. The presence of the constant term with the ToT technique may be due to small differences in the charge vs. ToT curves from block to block, and if so, can potentially be reduced.

To study the time resolution, it is first necessary to correct for slewing. The event time reference is obtained from the scintillator paddles and Cerenkov counters, and the curve of signal time vs. integrated charge from ToT is parameterized assuming that the signal shape is well described by the form $V(t) \propto t^a e^{-bt}$. The width of the signal time distribution in slices of charge gives a measurement of the time resolution. A fit to the measurements of σ_t vs. charge from ToT (4 mV threshold) for a single block gives $\sigma_t = 220 \text{ ps} / \sqrt{E [\text{GeV}]} \oplus 140 \text{ ps}$, where the constant term is assumed to be due to trigger jitter. This assumption can be tested by measuring the width of

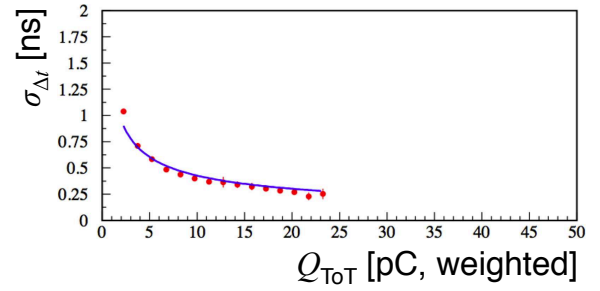


Fig. 10. Time resolution obtained using the ToT technique as a function of incident electron energy.

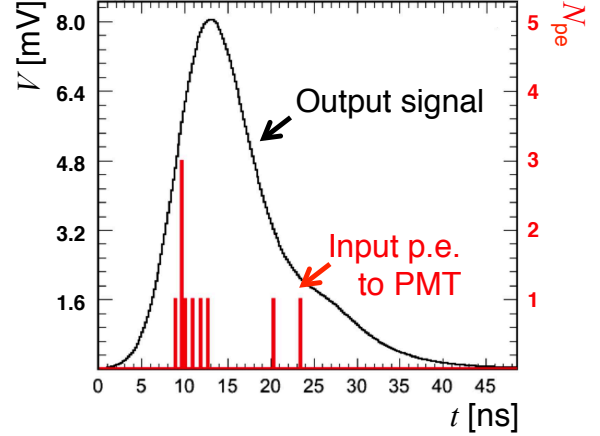


Fig. 11. Simulation of PMT signals. The red histogram shows the number of photoelectrons produced in bins of time (scale at right). The black curve is the resulting PMT signal (scale at left).

the distribution of signal time differences for two successive blocks. Assuming that the two blocks have the same intrinsic time response and that there is no common-mode contribution to the resolution, $\sigma_{t1} = p/\sqrt{E_1}$ and $\sigma_{t2} = p/\sqrt{E_2}$, so that we expect $\sigma_{\Delta t} = p/[E_1 E_2 / (E_1 + E_2)]^{1/2}$, with no constant term. Figure 10 shows the measurements of $\sigma_{\Delta t}$ in slices of the weighted charge measurements from ToT, $Q = Q_1 Q_2 / (Q_1 + Q_2)$ (4 mV threshold). The overlaid curve has $p = 210 \text{ ps}$ and no constant term, which is indicative of the intrinsic time resolution of the detector.

The results obtained at the beam test provide a point of comparison for the Monte Carlo (MC) simulation of the LAV system. The Geant4-based NA62 MC includes a detailed description of the LAV geometry and materials. Two sets of routines are available for shower simulation and the creation and propagation of Cerenkov photons: the standard Geant4 routines, with complete tracking of the optical photons, and our own routines, which make use of a response matrix obtained from the full simulation. In either case, the simulation produces the number of Cerenkov photons that arrive at the photocathode, together with their arrival times, as shown by the histogram in red in Fig. 11. A complete simulation of the PMT uses this information to generate an output signal, taking into account the PMT gain and transit-time fluctuations, the capacitance of the PMT, and dispersion in the readout cable. The resulting signal, which is illustrated by the black curve in Fig. 11, is input to a full simulation of the ToT discriminator,

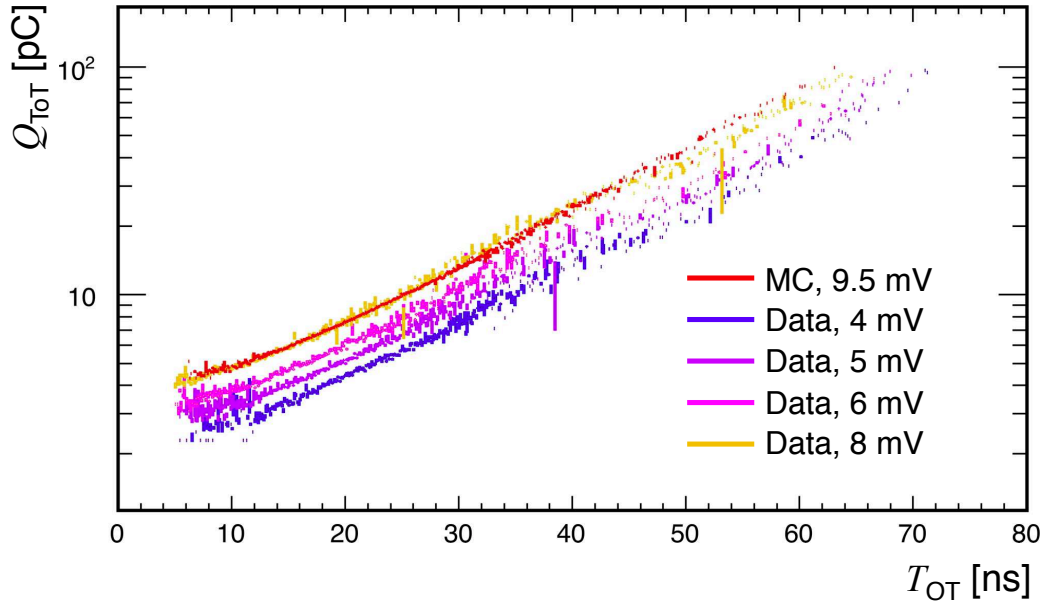


Fig. 12. Comparison of charge vs. ToT curves for MC (9.5 mV threshold) and data (various thresholds). Apart from a small discrepancy in the value of the threshold, the simulation accurately reproduces the shape of the charge vs. ToT curve.

including the comparator hysteresis. The complete simulation thus yields a description of the PMT signal, the integrated charge, and the ToT response.

Figure 12 shows charge vs. ToT curves for test-beam muons for four different threshold settings (4, 5, 6, and 8 mV). The red curve is from the simulation, with a threshold at 9.5 mV and all other adjustable parameters (e.g., tube gain, interdynode time fluctuations, PMT capacitance) set to typical or measured values. The simulation with a threshold of 9.5 mV accurately reproduces the shape of the measured charge vs. ToT curve with threshold 8 mV. Apart from this slight discrepancy, which is easily attributed to the accuracy of the manual threshold adjustment on the prototype ToT discriminator board, these results confirm our detailed understanding of the detector and the readout chain.

VI. STATUS AND OUTLOOK

Construction of the five small-diameter stations (including updating of the A1 prototype) was completed with all stations delivered to CERN and awaiting installation on the beamline in July 2011. Installation of these five LAVs is scheduled for December 2011. As of November 2011, construction of the remaining stations is in progress; the first of the intermediate diameter stations was recently completed (Fig. 13). Serial production of the front-end electronics boards is beginning. The installed detectors will be read out in a dry run in mid 2012, while a technical run with beam is scheduled for late 2012 and will include at least eight of the twelve LAVs. Data taking with the remaining detectors is planned for 2013.

ACKNOWLEDGMENTS

We warmly thank C. Capoccia and A. Cecchetti of the Experimental Apparatus Design Service (SPAS) at the INFN Frascati Laboratories, and S. Bianucci of INFN Pisa, for

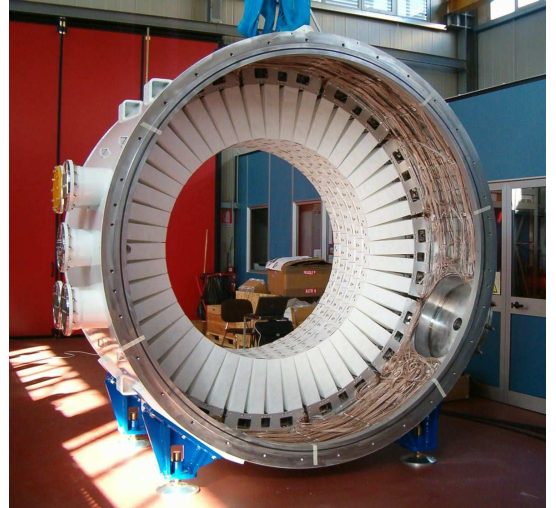


Fig. 13. The first intermediate diameter LAV station (A6) upon completion at Frascati in November 2011.

their collaboration on the mechanical design of the LAV system, including the steel vacuum vessels. We also thank our mechanical design team for their assistance in oversight of the construction of the steel vessels and of the transport of the completed detectors to CERN. We thank G. Corradi, D. Tagnani, and C. Paglia of the Electronics Service (SELF) at INFN Frascati for their collaboration on the design of the new HV dividers and front-end electronics boards. Construction was made possible by the contributions from our INFN technicians: E. Capitolo, R. Lenci, V. Russo, M. Santoni, T. Vassilieva, and S. Valeri (Frascati); F. Cassese and L. Roscilli (Napoli); L. Berretta and G. Petragani (Pisa); and F. Pellegrino (Roma). Finally, We thank V. Lollo and P. Chimenti of the Vacuum Service at INFN Frascati for their assistance with vacuum-related issues.

REFERENCES

- [1] V. Cirigliano *et al.*, 2011, in press, arXiv:1107.6001.
- [2] E949 Collaboration, A. Artamonov, *et al.*, *Phys. Rev. Lett.*, vol. 101, p. 191802, 2008.
- [3] F. Hahn (ed.) *et al.*, “NA62 technical design document,” 2010, NA62 Document 10-07.
- [4] OPAL Collaboration, K. Ahmet, *et al.*, *Nucl. Instrum. Meth. A*, vol. 305, p. 275, 1991.
- [5] F. Ambrosino *et al.*, in *2007 IEEE Nuclear Science Symposium Conf. Record*, Honolulu, Oct. 2007, pp. N05–6, arXiv:0711.3398.
- [6] A. Antonelli *et al.*, “The NA62 LAV front-end electronics,” 2011, in press.
- [7] B. Angelucci *et al.*, in *2011 IEEE Nuclear Science Symposium Conf. Record*, Valencia, Spain, Oct. 2011, pp. NP2.S–105.